Pranzas, K.P.; Boesenberg, U.; Karimi, F.; Muenning, M.; Metz, O.; Bonatto Minella, C.; Schmitz, H.-W.; Beckmann, F.; Vainio, U.; Zajak, D.; Welter, E.; Jensen, T.R.; Cerenius, Y.; Bormann, R.; Klassen, T.; Dornheim, M.; Schreyer, A.:

Characterization of Hydrogen Storage Materials and Systems with Photons and Neutrons

In: Advanced Engineering Materials (2011) Wiley

DOI: 10.1002/adem.201000298

Characterisation of Hydrogen Storage Materials and Systems with Photons and Neutrons**

By *P. Klaus Pranzas**, *Ulrike Bösenberg*, *Fahim Karimi*, *Martin Münning*, *Oliver Metz*, *Christian Bonatto Minella*, *Heinz-Werner Schmitz*, *Felix Beckmann*, *Ulla Vainio*, *Dariusz Zajac*, *Edmund Welter*, *Torben R. Jensen*, *Yngve Cerenius*, *Rüdiger Bormann*, *Thomas Klassen*, *Martin Dornheim* and *Andreas Schreyer*

[*] *Dr. P. K. Pranzas, Dr. U. Bösenberg, F. Karimi, M. Münning, O. Metz, C. Bonatto Minella, H.-W. Schmitz, Dr. F. Beckmann, Prof. Dr. R. Bormann, Prof. Dr. T. Klassen, Dr. M. Dornheim, Prof. Dr. A. Schreyer*
GKSS-Forschungszentrum Geesthacht GmbH
Max-Planck-Straße 1, D-21502 Geesthacht, Germany
E-mail: pranzas@gkss.de

Dr. U. Vainio, Dr. D. Zajac, Dr. E. Welter
HASYLAB/DESY, Notkestraße 85, D- 22607 Hamburg, Germany

Prof. Dr. T. R. Jensen
Interdisciplinary Nanoscience Center (iNANO) and Department of Chemistry, University of Aarhus, Ny Munkegade 118, DK-8000 Aarhus C, Denmark

Y. Cerenius
MAX-lab, Lund University, Ole Römers väg 1, SE-223 63 Lund, Sweden

[**] *The authors gratefully acknowledge Dr. Malte Oggureck, GKSS, for preparing the NCT image shown in figure 6 as well as Dr. Peter Staron, GKSS, for drawing the first version of the structural model shown in figure 7.*

Complex Hydrides are very promising candidates for future light-weight solid state hydrogen storage materials. The present work illustrates detailed characterisation of such novel hydride materials on different size scales by the use of synchrotron radiation and neutrons. The comprehensive analysis of such data leads to a deep understanding of the ongoing processes and mechanisms. The reaction pathways during hydrogen desorption and absorption are identified by in situ X-ray diffraction (in situ XRD). Function and size of additive phases are estimated using X-ray absorption spectroscopy (XAS) and anomalous small-angle X-ray scattering (ASAXS). The structure of the metal hydride matrix is characterised using (ultra) small-angle neutron scattering (SANS/USANS). The hydrogen distribution in tanks filled with metal hydride material is studied with neutron computerised tomography (NCT). The results obtained by the different analysis methods are summarised in a final structural model. The complementary information obtained by these different methods is essential for the understanding of the various sorption processes in light metal hydrides and hydrogen storage tanks.

1. Introduction

Photons and neutrons are powerful probes for the investigation of nanostructures and chemistry over the whole sample volume. Due to their different properties they offer complementary information. At neutron and synchrotron sources various techniques offer structural and chemical information on different time and length scales. *In situ* X-ray

diffraction (XRD) uses the high intensity of synchrotron radiation for fast *in situ* studies of the formation of crystalline phases.[1] X-ray absorption spectroscopy (XAS)[2] and anomalous small-angle X-ray scattering (ASAXS)[3] use the energy tunability of synchrotron radiation to get element specific information about oxidation state and structure sizes. In (ultra) small-angle neutron scattering ((U)SANS)[4] the strong interaction of neutrons with hydrogen is used to investigate hydrogen containing structures. With neutron computerised tomography (NCT)[5] the hydrogen distribution in tanks can be investigated due to the sensitivity of neutrons towards hydrogen and the large penetration depths of neutrons in matter.
Hydrogen is a very promising energy carrier for the future, especially for mobile applications. Light metal hydrides, like Reactive Hydride Composites (RHC),[6,7] can store hydrogen safely and reversibly at high volumetric densities. High requirements are posed on the reaction temperature, which is determined by the reaction enthalpy and the gravimetric storage as well as the reaction kinetics. In RHCs, the value of the reaction enthalpy is effectively lowered by an exothermic reaction with the formation of a new compound during the overall endothermic desorption reaction and vice versa for the absorption reaction.[8,9] A very prominent and promising system is $2\,LiBH_4+MgH_2 \leftrightarrow 2\,LiH+MgB_2+4\,H_2$ with a storage capacity of 11.5 wt%. The hydrogen sorption kinetics is distinctly improved by the addition of suitable transition metal compounds. A reduction in the reaction time by a factor of 10 is achieved by such additives in comparison to the pure composite material.[10]

In previous studies on MgH_2 based storage materials using small- and ultra small-angle neutron scattering (SANS/USANS), crystallite and particle sizes of the metal hydride were characterised showing the influence of hydrogen content and cycling history as well as the role of various additives and milling parameters.[11,12] The results indicated a crystallite coarsening as well as a break up of particles of radii larger than 10 µm during the cycling process.[11]
The chemical state and distribution of Ti-, Ni-, Zr- and V-based additives was characterised using XAS techniques[13,14] and ASAXS[15]. The information obtained by scattering techniques could be confirmed by TEM analysis exemplarily for Zr additives and a general model for the growth of MgB_2 and the role and function of transition metal based additives RHC was developed.[16]

For further optimisation of such hydrogen storage materials a deeper understanding of the sorption processes in the metal hydride matrix and the function of the additives is necessary.
Microstructural characterisation of such materials is extremely challenging because of their high reactivity and low stability. However, crystallite and particle size, microstructural distribution and orientation of the phases, both of the hydride matrix and the additives, are important parameters for the reaction kinetics and this information contributes significantly to the understanding of ongoing reactions and rate limiting processes.
In this article we present the results of the different analysis methods using synchrotron radiation and neutrons exemplarily for $LiBH_4$-MgH_2 composites with the Nb-based additive NbF_5. The strong interaction between neutrons and hydrogen is used to obtain tailored information on the phase distribution in RHCs with and without additive. Furthermore, neutron tomography of a hydrogen storage tank filled with $NaAlH_4$ / TiF_3 material is used to illustrate the hydrogenation behaviour and hydride distribution in a tank containing a complex metal hydride. The results of the different analysis methods demonstrate the potential of the two probes to fully characterize such complex processes occurring in novel hydrogen storage materials.

2.Experimental

$LiBH_4$, MgH_2, LiH, Al and MgB_2 powders and the additives NbF_5 and TiF_3 were purchased from Alfa Aesar and NaH from Sigma Aldrich with the highest available purity. For the investigations on the composites $LiBH_4$–MgH_2, the as received MgH_2 was pre-milled for 5 h in a Spex 8000M mixer mill. After this first high energy ball milling step, $LiBH_4$ and 10 mol % of the additive NbF_5 were added and milled for additional 5 h. For all milling experiments, a 50 ml hardened steel vial was used, a sample mass of about 5 g and a ball to powder ratio of 10:1 were selected. The $NaAlH_4$ / TiF_3 powder used for NCT studies of hydrogen tanks was produced by mixing the educts NaH, Al and TiF_3 on a roll bank for 12 h, milling under dry conditions for additional 12 h in a vibratory tube mill and conditioning at 125°C before starting with hydrogen absorption.[17] All handling and milling was performed under a continuously purified argon atmosphere.

In situ XRD measurements were performed in transmission mode at the instrument I711 at MAX-lab, Lund, Sweden.[18] The samples were mounted in single crystal sapphire tubes under argon atmosphere. The diffraction patterns were measured at an X-ray wavelength λ of 0.1072 nm using a MAR 165 CCD detector. The samples were heated by a tungsten wire below the capillary. The temperature was controlled by an inserted thermocouple and controlled by an external PID regulator. For details of the experimental setup, please see ref.[1].

The XAS investigations were carried out at the HASYLAB beamline C, DESY, Hamburg. The samples were mixed with cellulose and pressed into pellets of 13 mm in diameter which were mounted between Kapton tapes. The samples were measured in transmission mode in the energy range 18830 – 19440 eV at room temperature under vacuum conditions.

The ASAXS measurements were performed at the HASYLAB beamline B1 at DESY.[19] The RHC samples with 10 mol% of the additive NbF_5 were measured under vacuum conditions in 1 mm thick sample holders sealed by Kapton tapes. A low resolution XAS scan in the range of the K absorption edge of Nb (18986 eV) was measured prior to each ASAXS measurement to determine the exact position of the absorption edge of each sample. The sample transmission was determined by measuring the fluxes of direct and transmitted beam with photodiodes. The ASAXS intensities were measured at five different energies below the previously determined absorption edges. The sample to detector distances were 935 and 3635 mm. The scattering vector q ($q = 4\pi \sin\theta/\lambda$) is used as a measure of the scattering angle 2θ, where λ is the X-ray wavelength. The measured 2D data were corrected for dark current, detector response and sample transmission and were azimuthally integrated. Using pre-calibrated glassy carbon standards, the intensity was put on an absolute scale, that is the scattering cross section $d\Sigma/d\Omega$. The constant background due to resonant Raman scattering and fluorescence was subtracted from the scattering data. The resonant scattering of the Nb containing phase was separated using the method of G. Goerigk.[20] Distance distributions were calculated from the resonant scattering curves using the fit program GNOM.[21]

SANS experiments were carried out at the instrument SANS-2 of the Geesthacht Neutron Facility (GeNF) using distances between sample and detector of 1, 3, 9 m and a wavelength λ of 0.58 nm ($\Delta\lambda/\lambda = 0.1$) as well as of 21 m with $\lambda = 0.58$ nm and $\lambda = 1.16$ nm to cover the range of scattering vector q between 10^{-2} nm^{-1} and 3 nm^{-1}. Scattering data were normalised by monitor counts, corrected for sample transmission and detector response. The scattering cross section $d\Sigma/d\Omega$ was obtained using a vanadium standard. Ultra small-angle neutron scattering (USANS) experiments were performed at the double crystal diffractometer (DCD) at GeNF[22] with a wavelength of $\lambda = 0.443$ nm resulting in an accessible q range from 10^{-4} to 10^{-2} nm^{-1}.

For both, SANS and USANS investigations, the samples were measured in quartz cuvettes with a thickness of 1 mm. The scattering curves were obtained after desmearing and correction of multiple scattering according to the procedure described by Staron and Bellmann.[23] The SANS and USANS curves were combined to one curve for further analysis.

Neutron computerised tomography (NCT) investigations of a hydrogen tank, filled with nanocrystalline $NaAlH_4$ / TiF_3 powder, were performed after desorption and absorption of hydrogen at the neutron radiography and tomography instrument GENRA-3 at GeNF. The 165x165 mm large tank made of 40 mm manganese-strengthened aluminium has a sample thickness of 6 mm and is equipped with heating cartridges and temperature sensors. It was specified for an operating pressure of 100 bars and an operating temperature of 180 °C. After conditioning of the tank at 125°C, hydrogen was absorbed at the same temperature, at a pressure of 80 bar and at a slow hydrogen flow of first 25 and then 50 mL/min, regulated by an automatic mass flow controller. For desorption the temperature was 160°C and the flow was fast with several L/min. After the first absorption and desorption step a second complete absorption was performed. The NCT experiments were run with an L/D ratio of 150, a beam size of 24×24 cm^2 and a flux of $3.2 \cdot 10^6$ n $cm^{-2}s^{-1}$. A detailed description of the NCT setup can be found in ref.[5]. Here a CCD camera with 3056 x 3056 pixels, a chip size of 12 μm and a true dynamic range of 13 bit as well as a 50 mm lens was used.

2. Results and Discussion

3.1 *In situ* XRD

In these new and complex RHC materials, the reaction pathway as well as intermediate and side reactions cannot always be reliably predicted due to kinetic barriers and the lack of thermodynamic data. However, the exact knowledge of the ongoing reactions as a function of pressure and temperature is important. For the identification of the reaction pathway and the different crystalline phases forming during desorption and absorption of hydrogen, *in situ* XRD is a very powerful tool. Exemplary, such experiments performed on pure $LiBH_4$–MgH_2 composites are shown in figure 1.

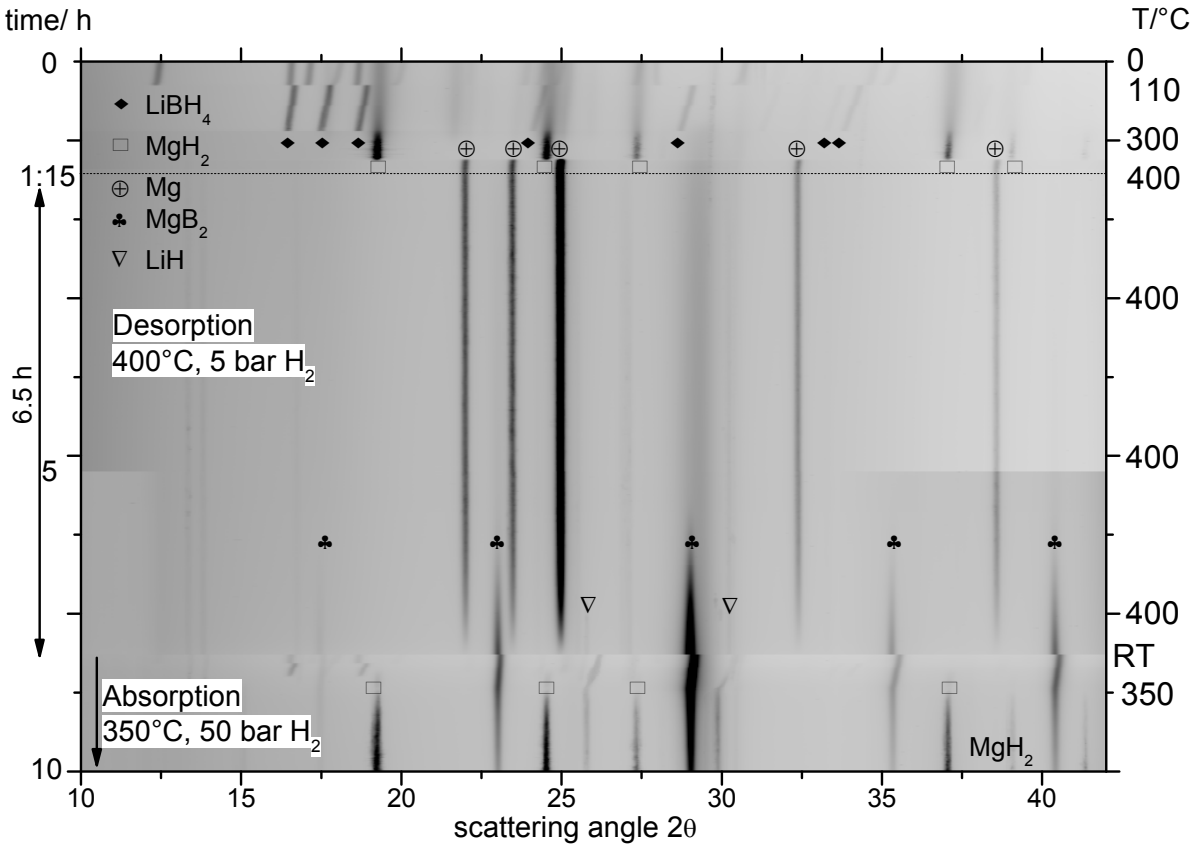

Fig. 1. In situ XRD measurement of pure $LiBH_4$–MgH_2 composites during hydrogen desorption, heating with 5 K/min to a final temperature of 400°C and holding isothermal under a pressure of 5 bar hydrogen, and absorption of hydrogen, under a pressure of 50 bar hydrogen at a temperature of 350°C with intermediate cooling to room temperature. The different phases are marked by symbols (see legend).

The as milled material is heated with a rate of 5 K/min to a final temperature of 400°C and held isothermally for 4 hours under a constant pressure of 5 bar hydrogen. During the heating period three distinct events can be observed. At approx. 110°C the phase transformation of $LiBH_4$ from orthorhombic to hexagonal occurs. At 275 °C the $LiBH_4$ diffraction peaks fade out because of the melting of this phase. At temperatures around 330°C desorption of hydrogen from MgH_2 occurs, this reaction is coupled to the formation of metallic Mg. During the end of the isothermal period the formation of MgB_2 is observed. In contrast to composites with transition metal additives,[10] an incubation period between the formation of metallic Mg and the formation of MgB_2 is observed in the isothermal period. Under the applied conditions, the decomposition of $LiBH_4$ is directly correlated to the formation of MgB_2.
The material was then cooled to be loaded with hydrogen and heated to a final temperature of 350°C with 10 K/min to be held isothermal. Clearly the decrease of the MgB_2 peaks and the simultaneous rise of the MgH_2 peaks can be observed. The formation of $LiBH_4$ cannot be traced with this method because of its liquid state. However, cooling the sample after this experiment to room temperature, $LiBH_4$ can be clearly identified. Thus, the experiment illustrates nicely the ongoing reactions and phase transformations as function of pressure and temperature.

3.2 X-ray absorption spectroscopy

With the addition of transition metal based additives the incubation period prior to the formation of MgB_2 can be overcome and the reaction rates are significantly increased. By means of XRD the additive phase can not be detected after ball milling of the materials or after cycling, which already indicates a very fine distribution and small cluster sizes. However, to understand the function of the additives and their role during the reaction, knowledge of the chemical state is essential. Independent of size and distribution, the oxidation state and the neighboring atoms of an element can be determined from the behaviour at the respective absorption edge of the transition metal. Thus, the chemical state of the additive NbF_5 in the RHC system MgH_2-$LiBH_4$ was studied with X-ray absorption spectroscopy (XAS). XANES (X-ray absorption near edge spectroscopy) data of as milled and cycled samples as well as of reference materials NbF_5 and NbB_2 are shown in figure 2.

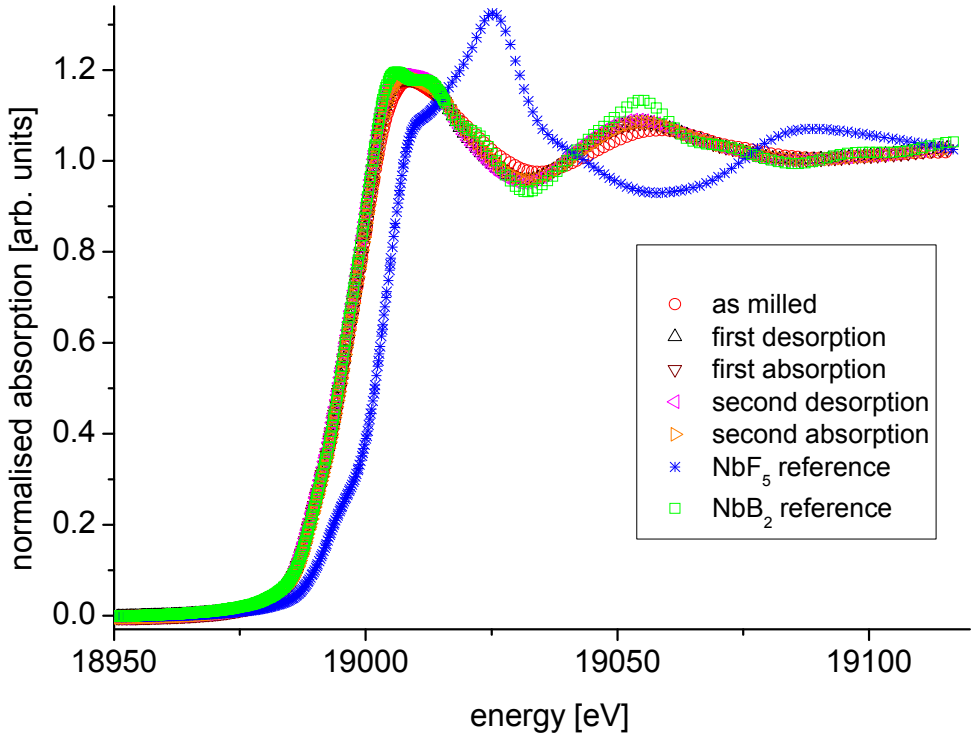

Fig. 2. XANES curves of NbF_5 doped $LiBH_4$-MgH_2 composites with different hydrogen cycling history in comparison to the reference samples NbF_5 and NbB_2.

The XANES curves of the RHC/ NbF_5 samples in figure 2 are different from the NbF_5 reference sample, but with proceeding cycling they coincide more and more with the curve obtained for NbB_2 reference material, regarding both the position of the absorption edge as well as the post edge oscillations. The post edge region contains information on the distance and type of the surrounding neighbouring atoms whereas the position of the edge is determined by the oxidation state.

This indicates that a large part of the NbF_5 additive in the RHC samples reacts to NbB_2 already during high energy ball milling. Further reduction takes place during the first sorption cycle. Upon further cycling the chemical state stays constant.

3.3 Anomalous small-angle X-ray scattering

Besides the chemical state, information on size and distribution of the additive phase is essential to understand its function. With anomalous small angle X-ray scattering (ASAXS) element specific information on its structures and cluster sizes can be extracted and ASAXS is therefore the method of choice to characterise the additive distribution in detail. Measuring at several energies in the vicinity of the absorption edge of the transition metal, the scattering and thus the information on size and structure of the additive phase can be extracted. The system of NbF_5 additive in RHC is shown here as example for a number of different additives analysed with ASAXS.[15] Figure 3 a) shows the separation of the resonant scattering of the Nb containing phase from the total scattering curve using the method of G. Goerigk.[20] Figure 3 b) displays the separated scattering curves of $LiBH_4$-MgH_2 composite samples with 10 mol% of the additive NbF_5 with different hydrogen cycling history, together with the corresponding fits (solid lines).

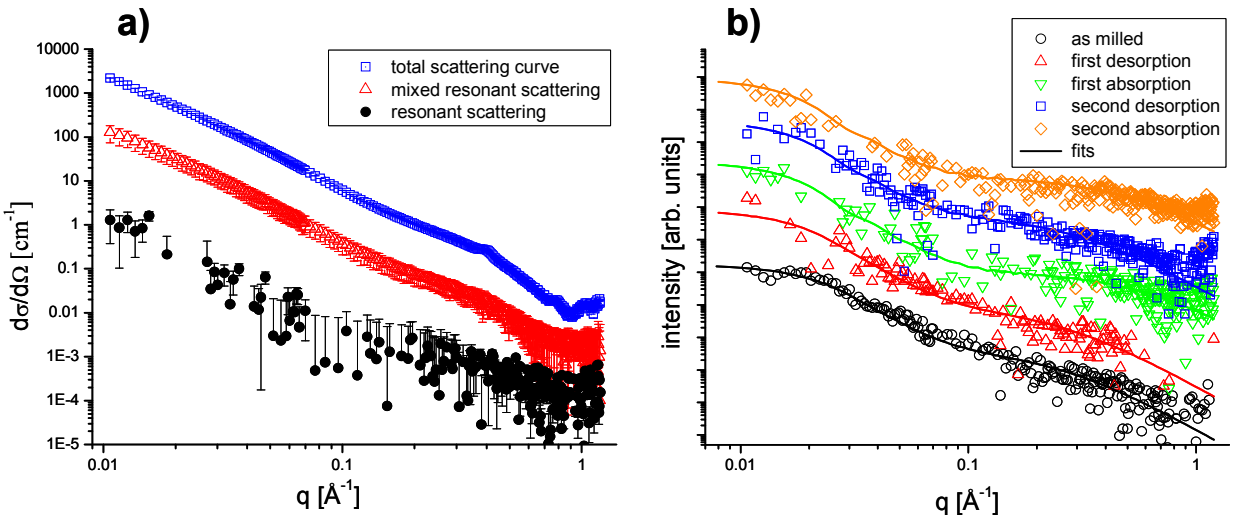

Fig. 3. ASAXS at the k-absorption edge of niobium: a) Separation of the resonant scattering of the Nb phase in $LiBH_4$-MgH_2 composites doped with NbF_5 after desorption and absorption of hydrogen. b) Separated resonant scattering curves of several NbF_5 doped $LiBH_4$-MgH_2 composite samples with different hydrogen cycling history. The curves are shifted for clarity. The solid lines are the fits obtained calculating the distance distributions shown in figure 4.

In figure 4 the distance distributions calculated from the separated resonant scattering curves shown in figure 3 b) using the fit program GNOM[21] are presented.

The most frequent sizes of niobium containing structures (maxima of the distributions) are for all cycles in the range of 10 – 15 nm. Largest Nb structures which are found in the RHC matrix are between 27 and 35 nm. For the as milled state the smallest structures are found. During the first desorption and absorption the structures are shifted to larger sizes and stay constant upon further cycling. The small coarsening effect of these structures during the first cycle seems to have no negative effect on the sorption kinetics.

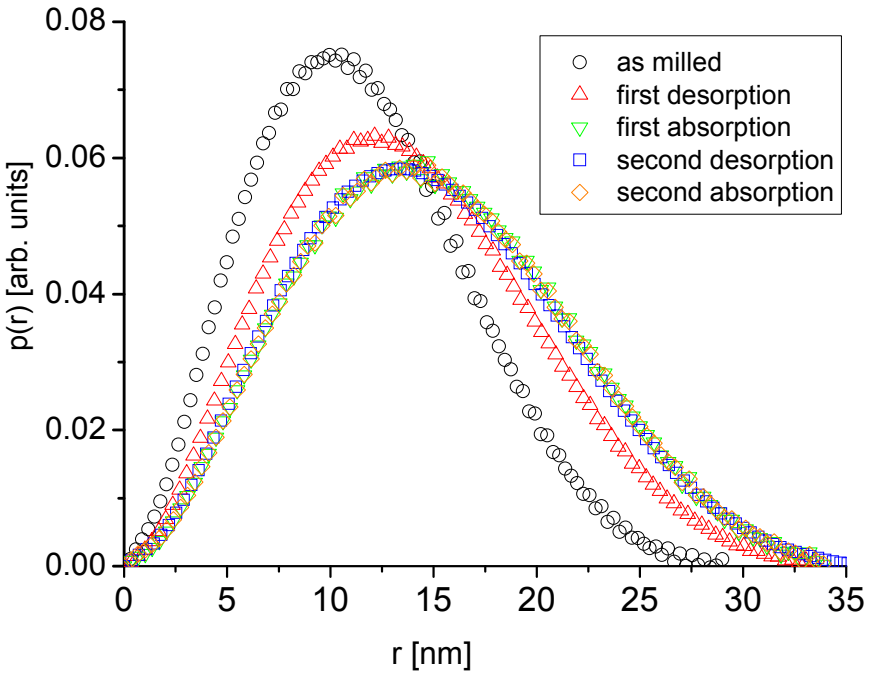

Fig. 4. Distance distribution curves with Nb containing structures as ASAXS results of $LiBH_4$-MgH_2 composites with 10 mol% of the additive NbF_5 with different hydrogen cycling history.

The formation of these small NbB_2 structures found by XAFS and ASAXS compare well to previous results obtained for Zr- and Ti-based additives[13,15] and therefore a similar mechanism is supposed to improve the sorption kinetics.

3.4 (Ultra) small-angle neutron scattering

The previous results illustrated the state of the additive in the composites, not however, how the microstructure of the hydride matrix is influenced by it. For this, the combination of small-angle and ultra small-angle neutron scattering (SANS/USANS) offers ideal means. The combined SANS-USANS curves of the $LiBH_4$-MgH_2 composites without additive and with 10 mol% NbF_5 are shown in figure 5 a). In figure 5 b) size distributions calculated from these curves using a two-phase model of spheres are presented.

The scattering curves show distinct differences at small and large q values which correspond to small and large radii in the size distributions, calculated using a simple hard spheres model (insert in figure 5). In these distributions the effects of the NbF_5 additive are clearly visible: For the sample with additive a smaller maximum radius significantly below 10 µm is obtained which reveals the formation of smaller particle sizes. The first maximum at about 1 nm shows that smaller structures like defects and small crystallites are formed in comparison to the RHC samples without additive.

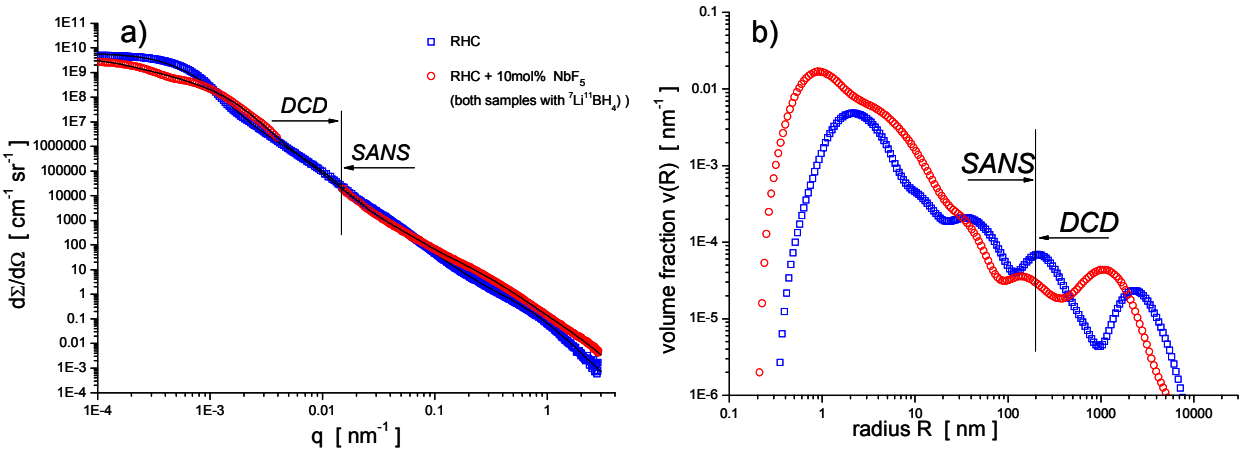

Fig. 5. a) Combined DCD (USANS) and SANS curves of RHC samples with and without NbF_5 additive after the second absorption with hydrogen. b) Corresponding calculated size distributions using a hard spheres model.

3.5 *In situ* neutron radiography and tomography

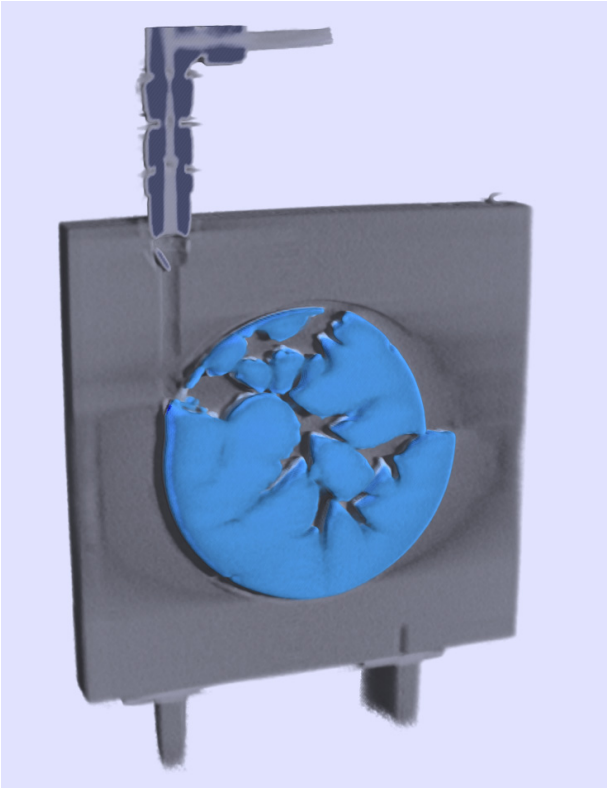

Fig. 6. NCT image showing the development of structures inside a hydrogen tank filled with the hydrogen storage material $NaAlH_4$ / TiF_3, after charging with approx. 20 L of hydrogen in a second absorption step.

Neutron computerised tomography (NCT) is a powerful method for studying the hydrogen distribution and hydrogenation behaviour in tanks filled with metal hydrides. In figure 6 the

NCT image of a hydrogen tank filled with the complex hydride $NaAlH_4$ doped with TiF_3 is shown. $NaAlH_4$ is considered a model system for the design and up scaling of complex light-metal hydrides because of its suitable sorption temperatures and kinetics but comparatively low storage capacity.

The NCT image in figure 6 illustrates the hydrogenation process inside a hydrogen tank filled with approx. 20 L of hydrogen after the three cycling steps activation (first absorption of hydrogen), first desorption and second complete absorption. A dendritic channel structure was formed in the metal hydride due to the compaction of the powder material at the high pressure of 80 bars. In parallel *in situ* neutron radiography investigations were performed (published elsewhere) which showed that this dendritic structure was formed immediately at the start of the first hydrogen absorption and the powder structure stayed stable during further cycling. During hydrogen absorption and desorption, a homogenous hydrogen distribution could be observed due to distinct changes in the colour of the metal hydride material.

4. Discussion

The results obtained by the different analysis methods for the matrix composite as well as for the TM-based additive can be summarised by a structural model, see figure 7. It illustrates how the powder particles consist of finer grains. A powder particle can well contain both phases of the composite. As revealed by XAFS and ASAXS a major part of the additive reacts to the corresponding boride already during high energy ball milling and forms nanostructures. The most straightforward and also confirmed position of the additives (for Zr-based additives[16]) is their location in the interphases and grain boundaries, this is illustrated by the zoom in figure 7.

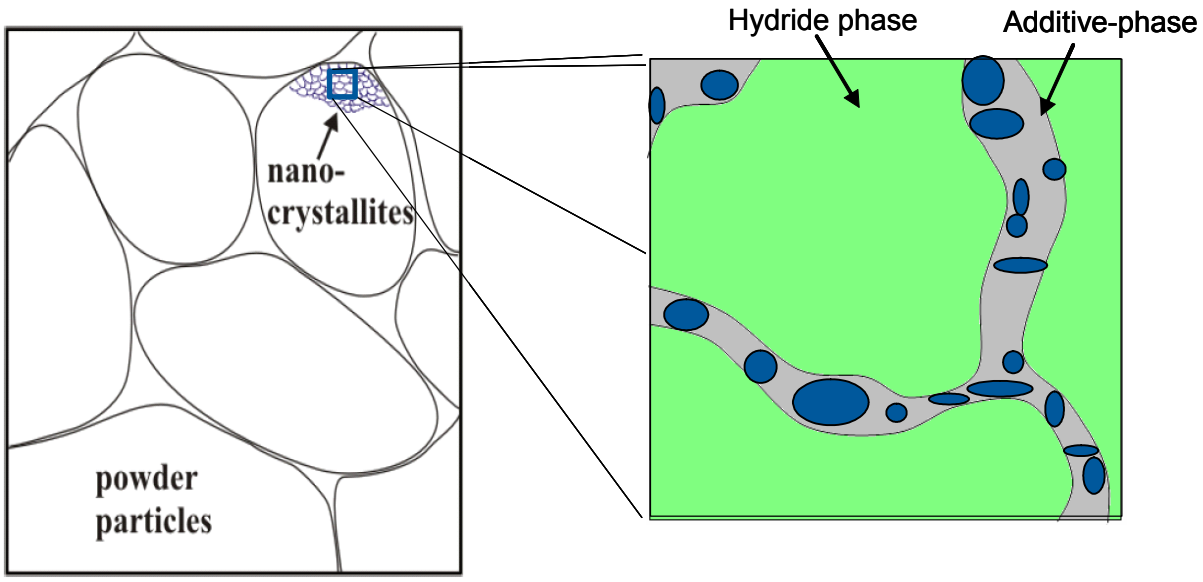

Fig.7. Structural model summarising all results obtained by the different analysis methods shown in this article (see text).

For NbF_5 as an additive, a similar mechanism and role is assumed as previously proposed for different transition metal based additive systems.[15,16] Transition metal borides like NbB_2 are thermodynamically very stable and thus chemically inert, an interaction with hydrogen and

therefore a catalytic role is not very likely. Because of the same crystal structure as MgB_2, a small lattice misfit between the two compounds can be assumed. Therefore NbB_2 might support heterogeneous nucleation and facilitate thereby the formation of MgB_2 during hydrogen desorption. Inoculation leads to an increase in reaction sites which refines the grain structure and displays faster sorption kinetics. This is leading to a larger number of reaction sites also during the absorption reaction and improves the reaction kinetics. As a result, the observed microstructure in presence of a transition metal based additive like NbF_5 appears refined after hydrogenation cycling in comparison to the composite without additive. The model is derived in detail in ref.[11,12,15,16], taking also the reaction kinetics, rate limiting processes, growth direction and orientation relationships of the different phases into account.
By SANS/USANS also smaller particle sizes were found in samples doped with NbF_5 in comparison to samples without additive. The obtained stable nanostructure with a large surface area resulting in a good kinetics is important for the cycling stability of a reversible hydrogen storage system.

The NCT measurements show the behaviour of loosely compacted hydrogen storage materials in a tank during hydrogen uptake. The formation of such dendritic channels in the powder bed due to the hydrogen flow is very unfavourable since it hinders the heat flux through the powder bed towards the tank cylinder wall. Furthermore, after several cycles the powder is expected to be collected more and more at the bottom of such a hydride tank cylinder. In that case huge compressive stresses could emerge locally due to the expansion of the crystal lattice due to hydrogen uptake which could cause tank fracture. This example illustrates the importance of the knowledge of the ongoing processes in the powder bed upon cycling.

5. Conclusions

Photons and neutron offer the possibility to study hydrogen storage materials and systems based on light metal hydrides on all size scales from the nanostructure up to complete hydrogen tanks. Information about the ongoing reactions as well as parameters influencing the reaction kinetics can be obtained, leading to a better understanding of these reactions and rate limiting processes. This information is essential for the development and further optimisation of this new type of hydrogen storage materials.
In addition, NCT allows for non-destructive investigations of complete hydrogen tanks filled with these materials. The information given by such measurements enables the design and optimisation of storage tanks with regard to efficiency and safety.

References

[1] D. Ravnsbæk, L. Mosegaard, J.E. Jørgensen, T.R. Jensen, *Proceedings of the 29th Risø International Symposium on Materials Science: Energy Materials – Advances in Characterization, Modelling and Application.* Risø National Laboratory for Sustainable Energy, Technical University of Denmark, **2008**, 349.

[2] M. Newville, in *Fundamentals of XAF*, University of Chicago, IL, **2008.**

[3] H. Stuhrmann, G. Goerigk, B. Munk, in *Handbook on Synchrotron Radiation*, , Elsevier Science, Amsterdam, The Netherlands **1991**, Ch. 17 (*Anomalous X-ray Scattering*).

[4] S.M. King, *Small Angle Neutron Scattering, in Modern Techniques for Polymer Characterisation*, (Eds: R. A. Pethrick & J.V. Dawkins), John Wiley, **1999.**

[5] F. Beckmann, J. Vollbrandt, T. Donath, H.W. Schmitz, A. Schreyer, *Nuclear Instruments and Methods in Physics Research* **2005**, A 542, 279.

[6] G. Barkhordarian, T. Klassen, M. Dornheim, R. Bormann, *J. Alloys Compd.* **2007**, 440, L18.
[7] G. Barkhordarian, T. Klassen, R. Bormann, Patent Pending, **2004**, German Pub. No 102004/061286.
[8] M. Dornheim, N. Eigen, G. Barkhordarian, T. Klassen, R. Bormann, *Advanced Engineering Materials* **2006**, 8, 377.
[9] M. Dornheim, S. Doppiu, G. Barkhordarian, U. Boesenberg, T. Klassen, O. Gutfleisch, R. Bormann, Viewpoint Paper, *Scripta Materialia* **2007**, 56, 841.
[10] U. Bösenberg, S. Doppiu, L. Mosegaard, G. Barkhordarian, N. Eigen, A. Borgschulte, T. Jensen, Y. Cerenius, O. Gutfleisch, T. Klassen, M. Dornheim, R. Bormann, *Acta Mater.* **2007**, 55, 3951.
[11] P. K. Pranzas, M. Dornheim, D. Bellmann, D., K.-F. Aguey-Zinsou, T. Klassen, A. Schreyer, *Physica B: Condensed Matter* **2006**, 385-386, 630.
[12] P. K. Pranzas, M. Dornheim, U. Bösenberg, J. R. Ares Fernandez, G. Goerigk, S.V. Roth, R. Gehrke, A. Schreyer, *J. Appl. Cryst.* **2007**, 40, S 383.
[13] E. Deprez, M. Muñoz-Márquez, M. Roldan, C. Prestipino, J. Palomares, C. Bonatto Minella, U. Bösenberg, M. Dornheim, R. Bormann, A. Fernandez, *J. Phys. Chem. C* **2010**, 114, 3309.
[14] J. Graetz, S. Chaudhuri, T.T. Salguero, J. J. Vajo, M. S. Meyer, F. E. Pinkerton, *Nanotechnology* **2009**, 20, 204007.
[15] U. Bösenberg, U. Vainio, U., P. K. Pranzas, J. M. Bellosta von Colbe, G. Goerigk, E. Welter, M. Dornheim, A. Schreyer, R. Bormann, *Nanotechnology* **2009**, 20, 204003.
[16] U. Bösenberg, J. W. Kim, D. Gosslar, N. Eigen, T. R. Jensen, J. M. Bellosta von Colbe, Y. Zhou, M. Dahms, D. H. Kim, R. Günther, Y. W. Cho, K. H. Oh, T. Klassen, R. Bormann, M. Dornheim, *Acta Materialia* **2010**, 58, 3381.
[17] N. Eigen, C. Keller, M. Dornheim, T. Klassen, R. Borman, *Scripta Materialia* **2007**, 56, 847.
[18] Y. Cerenius, K. Staal, L. A. Svensson, T. Usby, A. Oskasson, J. Albertson A. Liljas, *J Synchrotron Radiat.* **2000**,7, 203.
[19] H. G. Haubold et al, *Rev. Sci. Instrum.* **1989**, 60, 1943.
[20] G. Goerigk, *Europhysics Letters* **2004**, 66, 331.
[21] D. I. Svergun, *J. Appl. Cryst.* **1992**, 25, 495.
[22] D. Bellmann, P. Staron, P. Becker, *Physica B* **2000**, 276, 124.
[23] P. Staron, D. Bellmann, *J. Appl. Cryst.* **2002**, 35, 75-81.